Pergamon

0301-9322(95)00047-X

Int. J. Multiphase Flow Vol. 21, No. 6, pp. 1091–1106, 1995

0301-9322/95 $9.50 + 0.00

A PHYSICALLY BASED CORRELATION FOR THE EFFECTS OF POWER LAW RHEOLOGY AND INCLINATION ON SLUG BUBBLE RISE VELOCITY

P. S. CAREW[1], N. H. THOMAS† and A. B. JOHNSON[2]

[1]FAST Team, School of Chemical Engineering, University of Birmingham, Edgbaston, Birmingham, B15 2TT, England

[2]Schlumberger Cambridge Research Ltd, High Cross, Madingley Road, Cambridge, CB3 0HG, England

(Received 13 October 1993; in revised form 26 January 1995)

Abstract—A study has been made of the motion of long bubbles in inclined pipes containing viscous Newtonian and non-Newtonian liquids. A semi-theoretical expression for the rise velocity of air bubbles in water is derived on the hypothesis that the dominant factor is the momentum exchange of the bubble underflow, i.e. the bubble nose shape. The correlation calls on empirical inputs from established literature on bubble rise speeds at high Reynolds number. The effects of increasing Newtonian viscosity are analysed with reference to the momentum exchange and it is shown how viscosity reduces the inclination dependence of the bubble Froude number. Results from an experimental survey in seven different non-Newtonian liquids in three different diameter pipes are presented. These data are correlated so as to decouple the effects of surface tension and viscosity. An empirical relation is proposed for the effective shear rate in the fluid travelling around the bubble nose. Our correlation is compared to literature data from a broad range of Reynolds numbers with excellent agreement except at shallow angles.

Key Words: long bubbles, slug flow, non-Newtonian, inclination

1. INTRODUCTION

Over the past few decades much work has addressed the motion of long bubbles travelling in vertical, inclined and horizontal tubes. The vertical case is best understood and many theoretical and experimental papers are now available since the foundation studies of Davies & Taylor (1950) and Dumitrescu (1949). They carried out potential flow calculations based on an assumed spherical bubble nose shape. They derived theoretical Froude numbers very close to 0.35 which is now the accepted value for tubes greater than about 0.02 m in diameter (Reynolds number > 200, Eötvos number > 70), as confirmed experimentally by White & Beardmore (1962). Zukoski's (1966) survey of the effects of surface tension, viscosity and inclination not only confirmed the above result but also provided data to suggest that a limiting Froude number of about 0.5 exists for horizontal motion at high Reynolds and Eötvos numbers. Benjamin (1968) subsequently showed, theoretically, that the value is indeed 0.5 precisely for lossless planar flow and about 0.54 for pipes when a correction for the geometry is introduced. Couet *et al.* (1987) carried out planar inviscid calculations for the inclined rise of air bubbles. Their solution required that the contact angle at the bubble stagnation point was always $\pi/2$, even though a value of $\pi/3$ had previously been deduced by Stokes based on an analysis of the extreme shape of sharp crested water waves and was later used by Von Karman in his analysis of gravity currents (see Benjamin 1968). In fact, both of these are idealized prescriptions compared to real wetting behaviour. Nevertheless, their results agreed extremely well with the velocity and photographic data of Maneri & Zuber (1974). Couet *et al.* also suggested a formula for the Froude number at any inclination for Reynolds numbers $Re > 200$ and Eötvos numbers $Eö > 70$. Their calculation supposed limiting cases of vanishing surface tension effects, although Zukoski's (1966) inclined rise velocity data did not provide evidence that such a condition is typically attained.

†To whom all correspondence should be addressed.

Weber *et al.* (1986) investigated bubble rise in high viscosity Newtonian liquids and presented data for dependence of Froude number, Fr, on Eö and Mo (Morton number). A purely empirical attempt was made to correlate the values of Fr obtained with inclined pipes in terms of the limiting values of Fr for vertical and horizontal pipes. A reasonable fit was obtained, although there is some uncertainty with respect to their values assigned to the supposedly steady Froude number obtained in horizontal small tubes with viscosities as high as 6.12 Pa s. In viscosity dominated flow, the frictional retardation increases as the bubble propagates from the tube entrance, so the velocity should always decrease with increasing length of bubble. Presumably, in referring to horizontal Froude number, Weber *et al.* related their measurements to either nearly horizontal or to the starting Fr, or perhaps to bubbles of finite length.

Mao & Dukler (1991) used a two-equation (k–ϵ) turbulence model to calculate the flow field around a vertically rising Taylor bubble, arguing that such methods are often adequate in situations with little or no recirculation. However, these models do suffer from uncertainties relating to rapidly accelerated flow around the bubble nose and in formulating turbulence damping near the gas–liquid interface which Mao & Dukler assume identical to that at a solid boundary.

Our concern here is bubble behaviour in non-Newtonian liquids with particular reference to pseudoplastic properties. Niranjan *et al.* (1988) investigated mass transfer of gas from vertically rising Taylor bubbles in viscous Newtonian and non-Newtonian liquids. They used Wallis' (1969) relation for bubble speed assigning an apparent viscosity for their non-Newtonian CMC solutions based on a shear rate ($\dot{\gamma}$) equal to twice the ratio of bubble velocity to pipe diameter. Their comparison of measured and predicted rise speeds showed excellent agreement. However, this is not really surprising, as the power law indices, n, were at least 0.82 or, in other words, the effective viscosities (proportional to $\dot{\gamma}^{n-1}$) were only weak functions of $\dot{\gamma}$.

The experimental investigation presented here follows earlier methods reviewed above. Also, we propose an extension to Benjamin's (1968) theoretical approach, here incorporating the momentum exchange which equilibrates bubble motion in inclined flows. Scaling formulae are deduced for the rise velocity of air bubbles in water, based jointly on Zukoski's data and on a calculation of the drainage film behind the bubble nose where wall shear and gravitational forces are balanced. Rise velocity data for bubbles in non-Newtonian media are then correlated with the bubble Reynolds number as a correction to the air–water formula, using an effective shear rate which depends on both the pipe diameter and its angle of inclination.

2. MOMENTUM ANALYSIS FOR AIR BUBBLES IN WATER

Referring to figure 1(a) and (b) we can identify an integral momentum balance between stations far upstream and far downstream of the bubble nose. Our approach serves to focus attention on the momentum adjustment around the bubble nose [the "excess volume" of figure 1(a)] which must balance the bubble buoyancy in this region. Downstream of the nose [past Z–Z in figure 1(a)] the weight of draining film is balanced by wall friction and so has no effect on rise velocity. Point O in figure 1(a) is a stagnation point and the pressure is constant (here zero) everywhere along the interface. Assuming inviscid flow, it follows from Bernoulli's theorem that, referring to this datum, the pressure at the top of the tube cross-section far upstream is then given in terms of liquid density ρ and rise velocity u_1 by

$$p_0 = -\tfrac{1}{2}\rho u_1^2 \qquad [1]$$

with hydrostatic pressure variation across the flow section. The total pressure force, including the hydrostatic pressure acting over a section far upstream, is therefore

$$p_0 A + \rho g \frac{D}{2} A \cos\theta \qquad [2]$$

where D is the pipe diameter, A is the pipe cross-sectional area and θ is the inclination. Adding to this the momentum flux $\rho u_1^2 A$ gives the flow force (Benjamin 1968)

$$S_1 = \tfrac{1}{2}\rho u_1^2 A + \rho g \frac{D}{2} A \cos\theta \qquad [3]$$

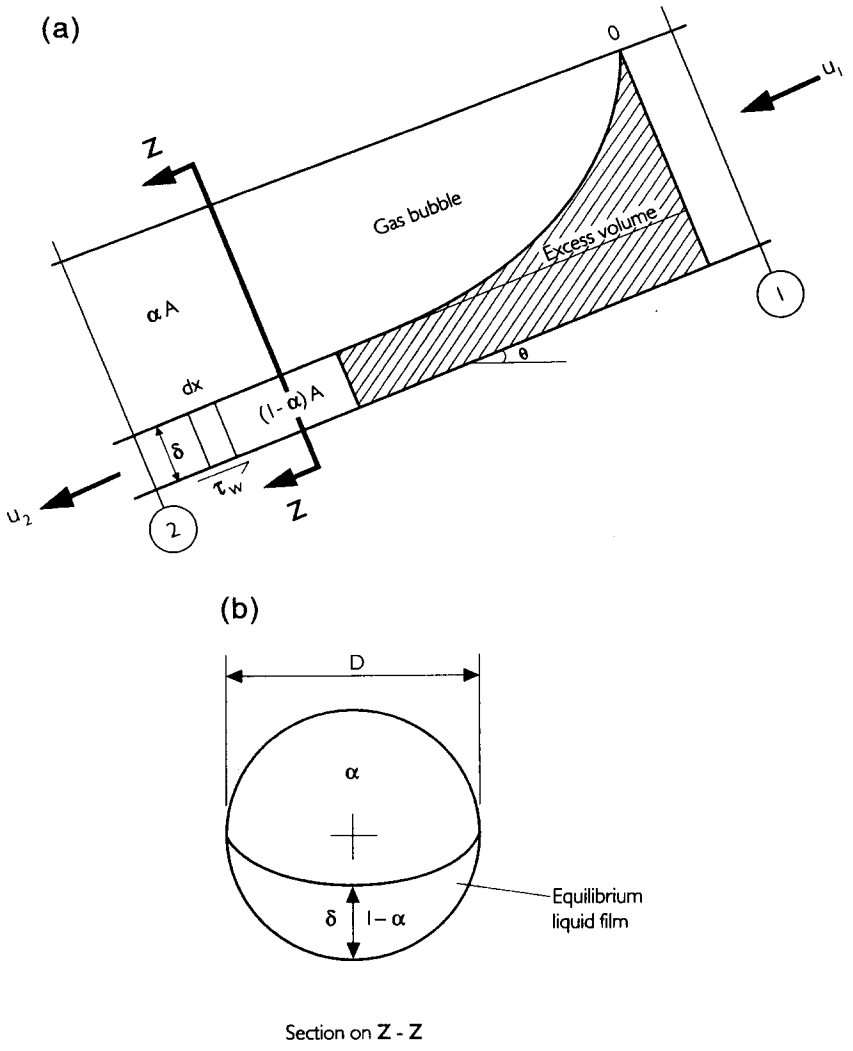

Figure 1. Schematic of an extended bubble rising in a closed, inclined, cylindrical tube.

The pressure variation is also hydrostatic at far downstream stations, from which it follows that the flow force here,

$$S_2 = \rho g \xi D \cdot \cos\theta \cdot [1 - \epsilon]A + \rho u_2^2 [1 - \epsilon]A \qquad [4]$$

where ξD is the distance between the interface and the centre of pressure in the film, i.e. following the approach outlined in the first part of the appendix, with

$$\xi = \frac{1}{2} - \epsilon + \frac{4\epsilon}{3\pi} \qquad [5]$$

This relation follows from an assumption that the liquid film sectional interface takes up a semi-elliptical form, as discussed further in the appendix. The axial momentum balance across the bubble nose region is then given by

$$S_2 - S_1 = \rho V g \cdot \sin\theta. \qquad [6]$$

Combining [3], [4] and [6] leads to

$$\rho u_2^2(1 - \epsilon)A + \rho g \cos\theta \cdot D\xi(1 - \epsilon)A - \left[\frac{1}{2}\rho u_1^2 A + \rho g \frac{D}{2} A \cos\theta\right] = \rho V g \sin\theta \qquad [7]$$

Continuity then requires

$$u_2 = \frac{u_1}{1-\epsilon} \qquad [8]$$

such that combining [5], [7] and [8] we obtain

$$\frac{V}{AD}\sin\theta = \frac{u_1^2}{gD}\cdot\left[\frac{1+\epsilon}{2(1-\epsilon)}\right] + \left[\epsilon^2\left\{1-\frac{4}{3\pi}\right\} + \epsilon\left\{\frac{4}{3\pi}-\frac{3}{2}\right\}\right]\cos\theta \qquad [9]$$

where $u_1^2/(gD)$ is the square of the bubble Froude number. Values for the downstream void fraction follow directly from considerations of continuity and the equilibrium between the resolved weight of the liquid film and the wall frictional force, together with Zukoski's (1966) data and our own air–water rise velocity data. At high Re the incremental increase in wall shear stress is less than at low Re. Since the depth of the equilibrium film is determined by a balance between resolved gravity and wall shear stress it follows that ϵ is a weak function of Re when Re is high. However, ϵ is strongly dependent on inclination, as displayed in the following correlation (figure 2), the development of which is described in the second part of the appendix:

$$\epsilon = 0.59 + 0.3031\left\{\frac{\theta}{90}\right\}^{0.2308} \qquad [10]$$

With this formula for ϵ, [9] then expresses the dependence of Fr on the fractional excess volume, $V' = V\sin\theta/AD$. The latter depends on inclination and surface tension and here we use Zukoski's data to calculate this dependence at high Reynolds number, as shown in figure 3. At 90° the value of V' is the same for all pipe sizes, which is not surprising since the Froude number is also the same for these high Reynolds number flows. The agreement demonstrates excellent compatibility between our momentum balance above and the experimental data. At the lowest incidence (1/2 degree) the points do not coincide, a disparity which we attribute to inadequacy of our approximation for the bubble shape in these limits (see appendix). Overall however, the behaviour broadly accords with our formula for the inclination dependence, especially with respect to the peak Froude numbers at θ between 45 and 60 degrees. All of these data are for water so surface tension is constant ($\sigma \sim 0.07$ N/m) and Eö ($=\rho g D^2/\sigma$) thus varies as the square of the pipe diameter. At high Eö the inertial forces dominate and the bubble nose underflow extends a greater distance downstream before achieving equilibrium film drainage flow. This corresponds to a visibly sharper bubble nose (Zukoski 1966), hence a greater value for V' and large Fr. Low Eö values correspond

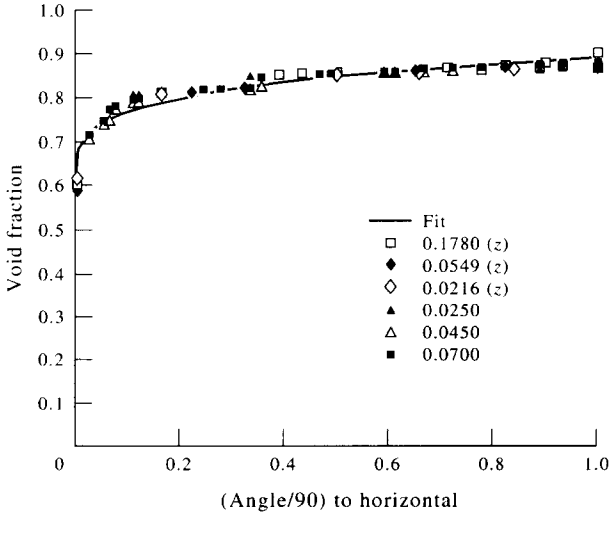

Figure 2. Variation of downstream cross-sectional voidage. Legend shows pipe diameter in metres.

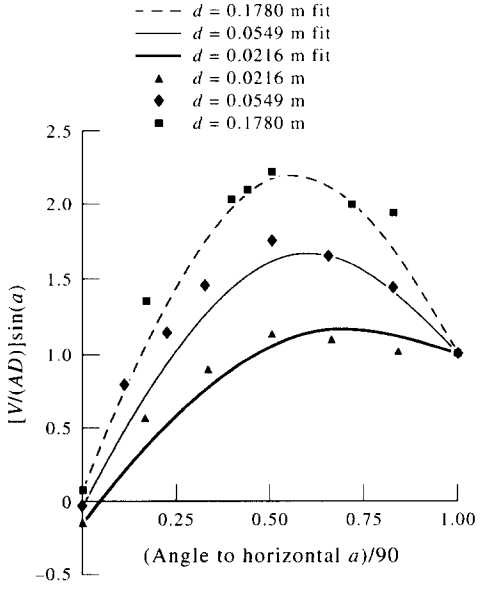

Figure 3. Non-dimensional, resolved excess volume variation with inclination angle (data from Zukoski 1966).

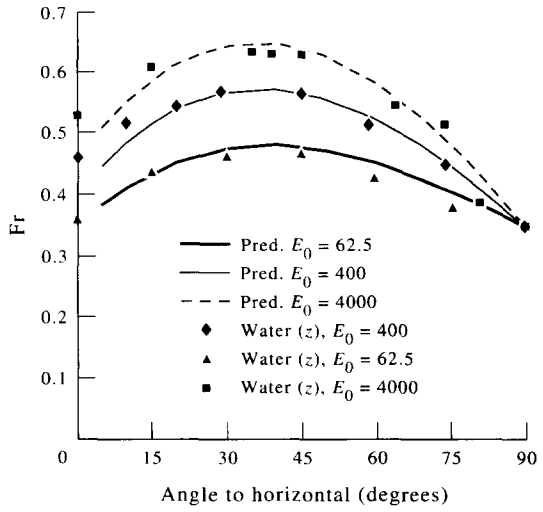

Figure 4. Comparison of Zukoski's (1966) air–water data with our correlation [15].

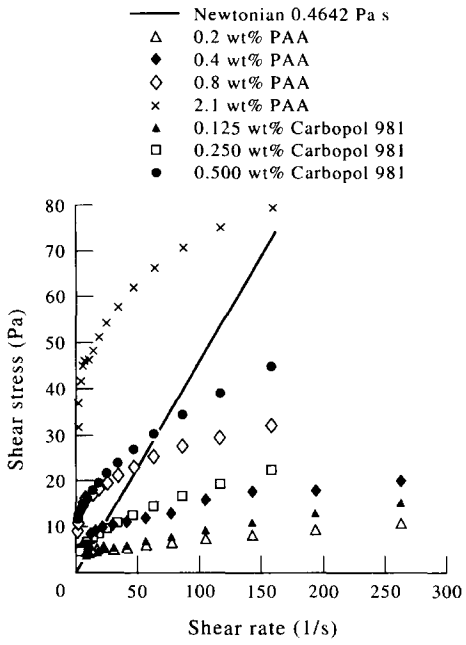

Figure 5. Shear stress vs strain rate data and power law fits for some of the solutions used in our experimental work.

to increased surface tension forces which cause the nose to become more rounded, resulting in reduced excess volume and Froude number.

Returning to figure 3, we note that V' behaves approximately as the sum of a sinusoidal variation and a linear trend. That is, for empirical correlation purposes:

$$\frac{V}{AD}\sin\theta = a\cdot\sin 2\theta + m\left[\frac{\theta}{90}\right] + c \qquad [11]$$

Surface tension dependence can be incorporated in this representation, according to which there is the following least squares fit for the coefficients:

$$a = 8.347[\log_{10}\text{Eö}]^{0.2} - 8.359 \qquad [12]$$

$$m = -0.164\log_{10}\text{Eö} + 1.555 \qquad [13]$$

$$c = 0.164\log_{10}\text{Eö} - 0.463. \qquad [14]$$

To sum up, we now have from [9] the Froude number

$$\text{Fr} = \frac{u_1}{\sqrt{gD}} = \sqrt{\frac{2(1-\epsilon)}{(1+\epsilon)}\left[\frac{V}{AD}\sin\theta - \left[\epsilon^2\left(1-\frac{4}{3\pi}\right)+\epsilon\left(\frac{4}{3\pi}-\frac{3}{2}\right)\right]\cos\theta\right]} \qquad [15]$$

which with [10] and [11]–[14] provides a simple physically-based formula for rise velocity in water when Eö > 60. Figure 4 confirms how well the correlation reproduces Zukoski's data for all inclinations.

Table 1. Physical properties of polymer solutions

Liquid name	Conc. (wt%)	Surface tension (N/m)	Approx. density (kg/m^3)	Consistency factor K (S.I. units)	Pseudo-plasticity index, n
Carbopol 981 with modified pH	0.5	0.077	1000	8.204	0.318
	0.25	0.077	1000	2.927	0.386
	0.125	0.0765	1000	1.016	0.485
Polyacrylamide	2.1	0.076	1000	30.158	0.1901
	0.8	0.075	1000	8.526	0.2646
	0.4	0.076	1000	3.127	0.3406
	0.2	0.0755	1000	1.6704	0.3307

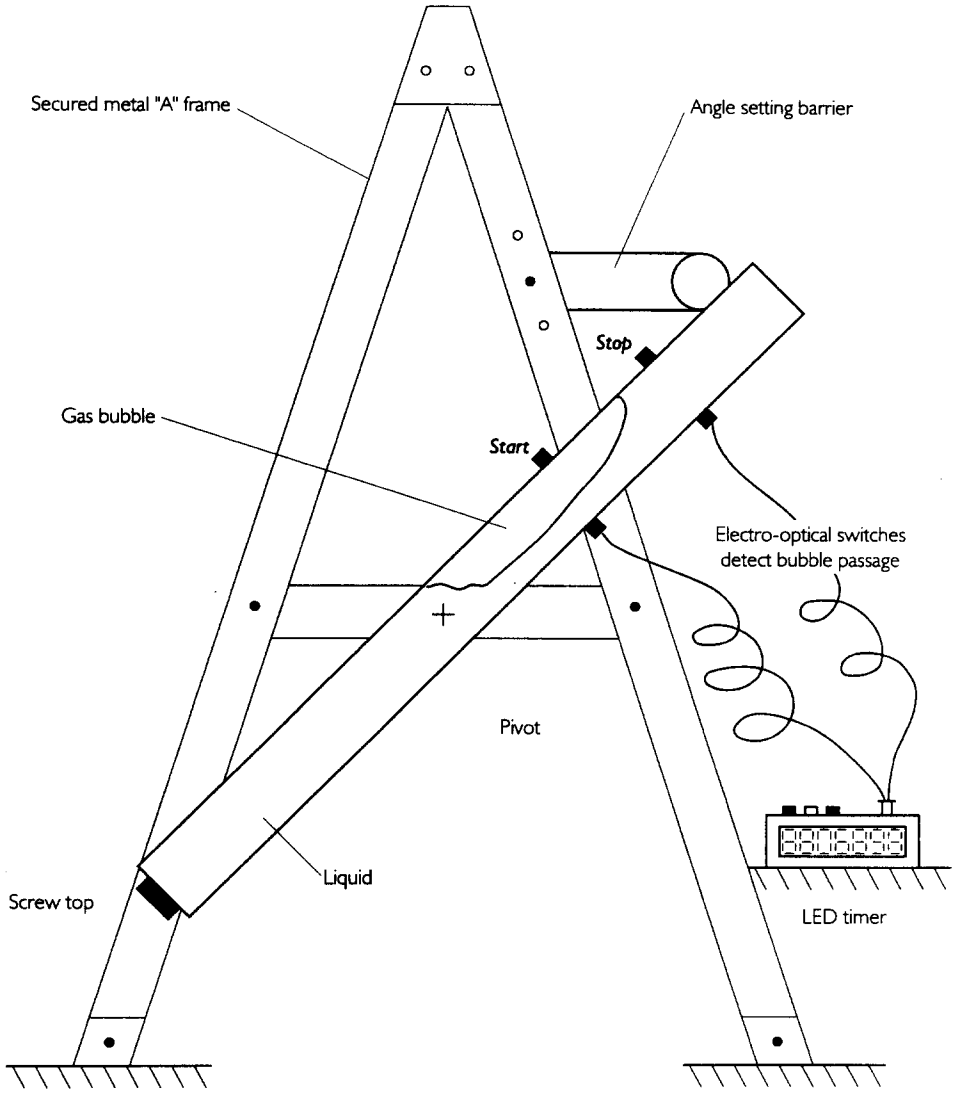

Figure 6. Tilting tube experimental apparatus for measurement of the rise velocity of single large bubbles in different tubes for all inclinations.

3. EXTENSION TO NEWTONIAN EFFECTS

To examine low Reynolds numbers effects, we must decouple the influence of viscosity μ and surface tension σ. This can be achieved in terms of the scale ratio

$$F = \frac{\mathrm{Fr}(\mathrm{E\ddot{o}}, \theta, \mathrm{Re})}{\mathrm{Fr}(\mathrm{E\ddot{o}}, \theta, \infty)} \qquad [16]$$

versus Re. For Re less than about 3, Zukoski's data ($\theta > 30$ degrees) were well described by Wallis' (1969) empirical relation for vertical tubes ($u_1 = 0.01\rho g D^2/\mu$). Assigning Taylor's asymptotic Fr (Eö, 90, ∞) = 0.35, Wallis' correlation can then be expressed as

$$F = 0.2857\sqrt{\mathrm{Re}} \quad \text{for} \quad \mathrm{Re} < 3. \qquad [17]$$

Wallis suggested an upper limit of Re < 1/2 but the data summary presented later (section 6) shows the approximation is sound up to Re $\approx$ 3.

Weber *et al.* (1986) presented data for air bubbles in a 0.0221 m diameter tube containing 100% corn syrup (viscosity 6.12 Pa s) for which Fr only varied from 0.03 to 0.04 for θ ranging from 10 to 90°. The corresponding Reynolds number was about 0.08. Wallis' correlation, based on data

for vertically rising bubbles, provides Fr $\approx$ 0.03. Inspection of other data (Runge & Wallis 1965) shows that as viscosity is increased the Fr ratio peak value to vertical value is decreased. Clearly, if the correlation holds for a broad range of inclinations then the explanation must be that V' remains essentially constant. This means that as θ reduces V must increase in a rather precise fashion to compensate for the reduction in the axial buoyancy.

4. EXPERIMENTAL EXTENSION TO NON-NEWTONIAN FLUIDS

A simple tilting tube rig, as described below, was used to measure the variation of bubble rise velocity with respect to pipe diameter, inclination angle and rheological properties. The polymers used were Carbopol 981 (BF Goodrich) and polyacrylamide (DP9-2530, Allied Colloids). These powders were dissolved in water to produce solutions with concentrations ranging from 0.125 to 2.1 wt%. A small amount of 1 M NaOH solution was added to achieve transparency of the Carbopol solution at pH 7. This modified the rheology somewhat, introducing a yield stress and generally thickening its consistency and apparently increasing visco-elasticity (a Weissenberg effect was observed during preparatory mixing when NaOH was added). The rheological parameters were measured with a concentric cylinder rheometer (Contraves) and surface tension with a Wilhelmy plate tensiometer (Whites Ltd). Density was taken to be that of water for all the solutions since water content was generally higher than 98%. Moreover, for the thicker liquids at low shear rates, tiny bubbles become trapped due to the high viscosities and/or yield stresses and these made density measurement difficult. Table 1 and figure 5 show physical properties, power law constants and rheograms.

The simple apparatus is shown in figure 6. Tubes of various diameters (0.025, 0.045 and 0.07 m) are attached to a metal frame which is pivoted centrally. The tubes are partially filled with test solution, leaving an air gap sufficient to supply the test bubble and then sealed with a screw cap. The test bubbles were all sufficiently long that their rise velocities were sensibly independent of length. The tube is rapidly rotated manually to the required inclination angle and the bubble rise velocity is measured. This is done automatically by a digital timer triggered through the interruption of two infra-red beams placed a known distance apart on the top quarter of the tube. Tests were carried out using a number of different detector intervals and axial positions, to confirm the bubbles rapidly (<5 diameters of travel) attained equilibrium velocity. Before each run the tubes were thoroughly cleaned with salt water, detergent, distilled water and acetone, thereby ensuring removal of surfactant impurities. The rise velocity was measured ten times for any one combination of pipe, fluid and inclination, providing Froude number measurements with repeatability to within 2%. Experiments with the most concentrated (2.1 wt%) polyacrylamide solution in the smaller diameter tubes showed that there was an extra slight (1–2%) effect on bubble velocity between consecutive tests under nominally identical conditions. To minimize this thixotropic effect, each reading was taken after the fluid had been sheared twice by previous bubbles and following a stagnant period of a few minutes thereby ensuring that the recent shear history of the fluid was the same in all cases. A more detailed description of the experimental technique is given in Carew (1993).

5. DISCUSSION OF EXPERIMENTAL RESULTS

Figures 7 to 12 show Fr versus θ for fixed Eö in seven different non-Newtonian liquids and three different pipes. All the data points follow the same basic trend, namely, that as the inclination angle is reduced from 90 degrees, the Froude number first increases, reaching a maximum at between 70 and 30 degrees inclination and then falling as θ approaches zero. We recall from section 1 that the inviscid case defines limiting values for vertical and horizontal Froude numbers. Indeed, with the more dilute solutions in the 0.07 m pipe (Eö $\approx$ 630) there is a striking similarity between the basic trend for low viscosity Newtonian data (water; see figure 4) and the present data (say 0.125 wt% Carbopol; see figure 9). Figure 7 displays low Eö (small diameter) data and reveals a similarity between viscous Newtonian data (section 3) and non-Newtonian data in terms of the ratio of peak to vertical Froude numbers. In all cases, Fr increases as inclination is reduced from 90 degrees and at a rate which is governed by concentration. As in the Newtonian case,

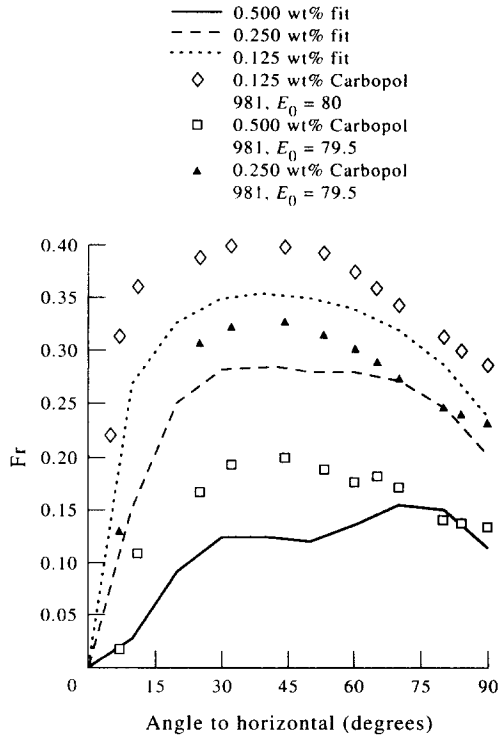

Figure 7. Rise velocity data and our empirical relation for a 0.025 m tube containing Carbopol 981 solution.

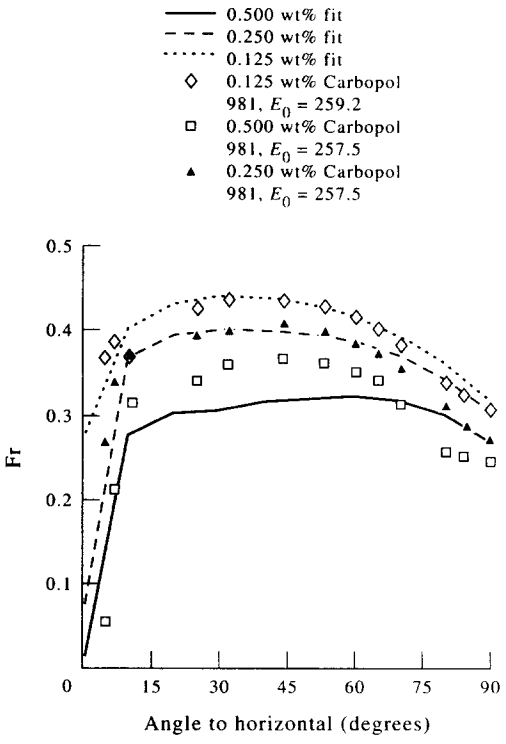

Figure 8. Rise velocity data and our empirical relation for a 0.045 m tube containing Carbopol 981 solution.

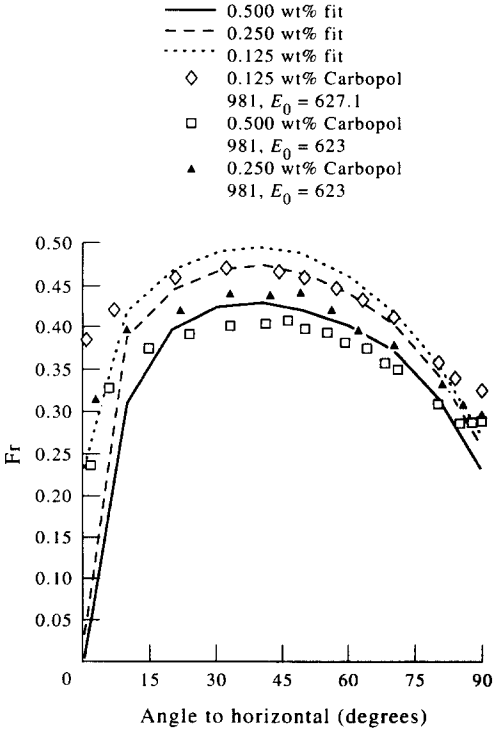

Figure 9. Rise velocity data and our empirical relation for a 0.07 m tube containing Carbopol 981 solution.

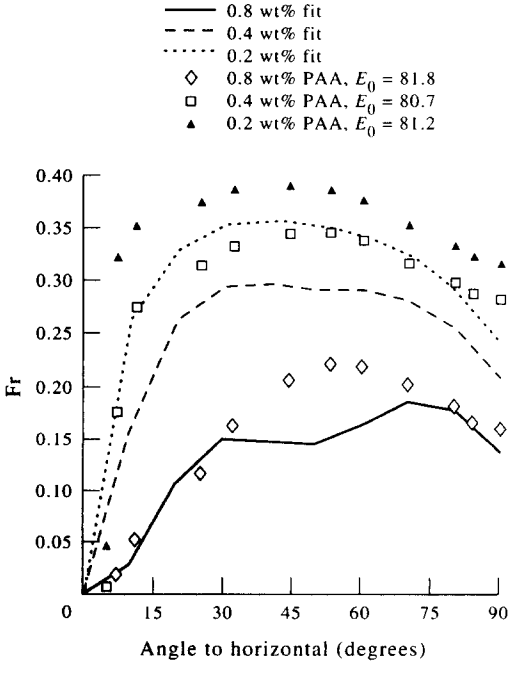

Figure 10. Rise velocity data and our empirical relation for a 0.025 m tube containing polyacrylamide solution.

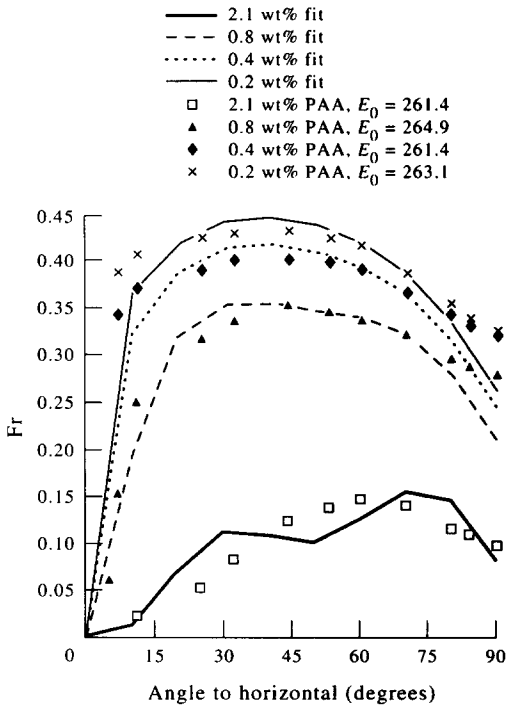

Figure 11. Rise velocity data and our empirical relation for a 0.045 m tube containing polyacrylamide solution.

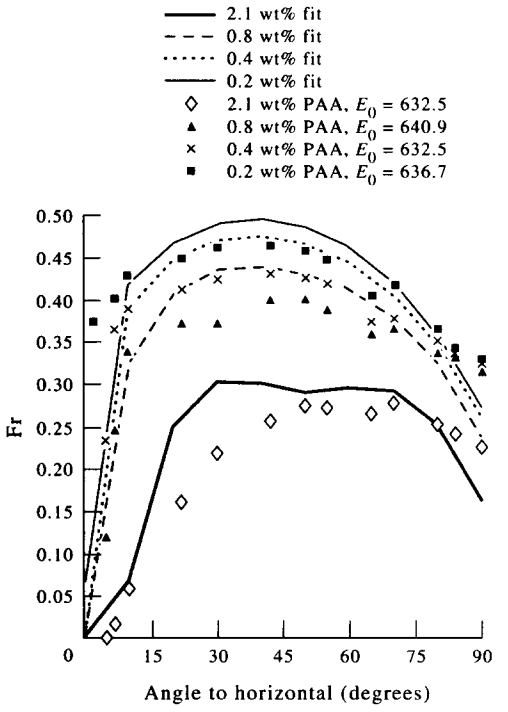

Figure 12. Rise velocity data and our empirical relation for a 0.07 m tube containing polyacrylamide solution.

Fr dependence on inclination is reduced as viscous effects become more important. Figures 8 and 9 show an altogether more Newtonian (high Re) response as compared with figure 4, except for angles lower than about 30 degrees. The low angle behaviour is better illustrated with reference to figures 10–12. Figure 10 shows how increasing polymer concentration results in decreasing

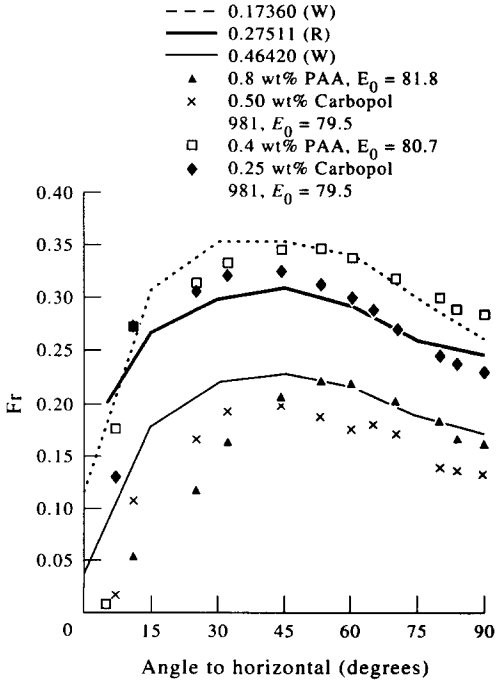

Figure 13. Comparison between some of our non-Newtonian data and literature Newtonian data for a roughly constant Eö value (67 < Eö < 82).

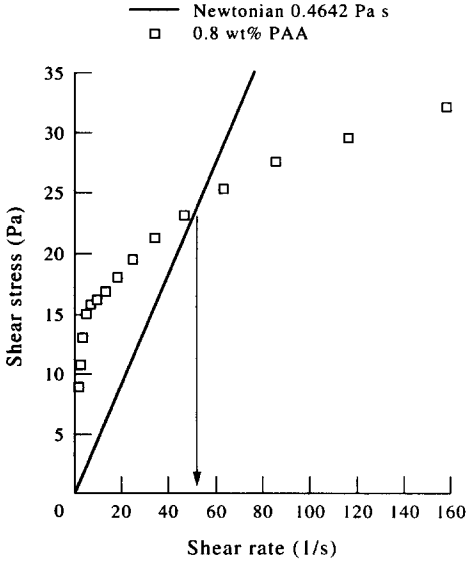

Figure 14. Close-up of rheological behaviour for rise velocity data sets coincident on figure 13.

Froude number such that the bubble rise speed rapidly approaches zero at inclinations close to horizontal. Moreover, increasing concentration (viscosity) amplifies the reduction in Fr. For example, a comparison of figures 4 and 10 shows that inclination has to be as high as 45 degrees before Fr variation with θ follows a similar trend to that observed with water. Note, also, that the angle above which Fr variation mimics that found with water reduces as the polymer concentration reduces or the pipe diameter and Eö increases (figures 11 and 12). At shallower inclinations, the rheological forces begin to dominate causing Fr to approach zero rather than some finite value as θ tends to zero. This phenomena of viscosity and rheology induced departure from the high Re trend at low angles can further be explained with reference to figures 13 and 14, as follows.

Figure 13 compares our non-Newtonian data with Newtonian data from literature sources ($75 < \text{Eö} < 82$). The clearest illustration of non-Newtonian effects is given by contrasting the present results for 0.8 wt% PAA with Weber *et al.*'s (1986) data for 0.4642 Pa s viscosity. For θ between 50 and 90 degrees, the two sets coincide almost exactly. This suggests that the non-Newtonian fluid is sheared at the same rate independent of angle and so flows with a constant viscosity. However, for $\theta < 50$ degrees the axial component of the "excess weight" rapidly falls with decreasing θ, causing a reduction in Fr and hence also a reduction in the effective shear rate. Figure 14 compares the rheologies of these two fluids and we note that for shear rates of less than 50 reciprocal seconds, the 0.8 wt% PAA has an apparent viscosity which significantly exceeds that of the Newtonian liquid. Interestingly, this intersection occurs at a point below which shear stress variation with shear rate is most pronounced. As shear rate increases, the ratio of shear stress to shear rate (apparent viscosity) continues to fall at an ever decreasing rate. In other words, for shallow angles velocities and shear rates are low and viscosities are high, whereas at steeper inclinations velocities and shear rates are increased and viscosities decreased allowing inertially dominated flow to occur (figure 4). Enlarging the pipe diameter causes an increase in Eö and Fr is also increased, causing an increase in shear rate. Figure 12 shows how rise data for 0.8 wt% PAA in a 0.07 m tube follow curves which resemble Newtonian equivalents even at angles as low as 10 degrees.

The general implication, then, is that at steeper inclinations and in larger pipes, the shear behaviour around the bubble nose can probably be adequately represented by an "effective" or "apparent" viscosity because the strain rate in the bubble nose zone is located in the upper part of the rheogram. At lower angles and in smaller pipes the behaviour is governed by the liquid rheology and the bubble rise speed rapidly approaches zero as inclination vanishes. As shown in table 1, we have fitted our rheograms with a power law. However, figure 5 shows that the more concentrated solutions could be well represented by a yield stress constitutive equation such as the Herschel–Bulkley model (Skelland 1967):

$$\tau = \tau_y + R\dot{\gamma}^s \qquad [18]$$

where τ and τ_y are shear stress and yield stress respectively and R and s are power law type constants, noting that the presence of a "true" yield stress can only be determined through detailed measurements at extremely low shear rate (Nguyen & Boger 1992). The effect of a yield stress in the smaller tubes could be to arrest bubble motion at some critical inclination. Indeed the results for 0.5 wt% carbopol on figure 13 indicate that the bubble might be arrested at $\theta \approx 5$.

6. CORRELATION FOR NON-NEWTONIAN BEHAVIOUR

To account quantitatively for non-Newtonian behaviour we return to the correlation approach described in sections 2 and 3 and again seek to decouple the viscous and surface tension effects. In figure 15, the scaling factor F (from [16]) for all earlier data is plotted versus Reynolds number based on the apparent viscosity associated with bubble strain rate, i.e. now dependent on pipe size and inclination angle. The apparent viscosity used here was assigned as follows. Firstly, we supposed that the effective shear rate $\dot{\gamma}_{\text{eff}}$ around the bubble scales as u_t/D. Secondly, we introduced a purely empirical factor to incorporate inclination effects, in particular, so as to force-fit the data for $\theta = 10$, 30, 45, 60 and 90 degrees to the established scalings for Newtonian fluids (see [17]).

The resulting expression for shear rate, namely

$$\dot{\gamma}_{\text{eff}} = \frac{u_1}{D}\left[122\left(\frac{\theta}{90}\right)^{3/2} - 443\left(\frac{\theta}{90}\right)^{5/2} + 572\left(\frac{\theta}{90}\right)^{7/2} - 232\left(\frac{\theta}{90}\right)^{9/2}\right] \quad [19]$$

represents an empirical correlation which provides a practically useful interpolation over all inclinations $\theta \geqslant 10°$.

The non-Newtonian Reynolds number can be expressed as

$$\text{Re} = \frac{\rho u_1 D}{K(\dot{\gamma})^{n-1}} \quad [20]$$

where K and n are the power law constants given in table 1. For this comparison, figure 16 shows [17], all our data for 90 degrees and Brown's (1965) semi-empirical equation for vertical flow:

$$\left[\frac{\text{Fr}}{\text{Re}}\right]^{2/3} \cdot \sqrt{1 + 8\left[\frac{\text{Fr}}{\text{Re}}\right]^{-2/3}} - \left[\frac{\text{Fr}}{\text{Re}}\right]^{2/3} + 4\left[\frac{\text{Fr}}{0.35}\right]^2 - 4 = 0 \quad [21]$$

also given in figure 15. This equation holds for

$$\text{Re} > \text{Fr} \cdot \sqrt{\left(\tfrac{15}{2}\right)^3} \quad [22]$$

and we only show the valid portion on figure 16.

In discussing the implications of figures 15 and 16, it is helpful to distinguish the following ranges of Re.

(a) Re > 1000

In this range the inertial forces dominate for all inclinations. F tends to 1 as $\text{Re} \to \infty$ and [10]–[15] are a good approximation even for rheologically complicated liquid phases.

(b) Re < 3

Here the correlation approximates to the empirical expression of Wallis (1969), now generalized to recognize that an appropriate effective shear rate expression must be incorporated to give the apparent viscosity. The flow around the bubble is laminar and shear rates are low everywhere. The liquid constitution resides in the highly non-linear region of the rheograms shown in figure 5.

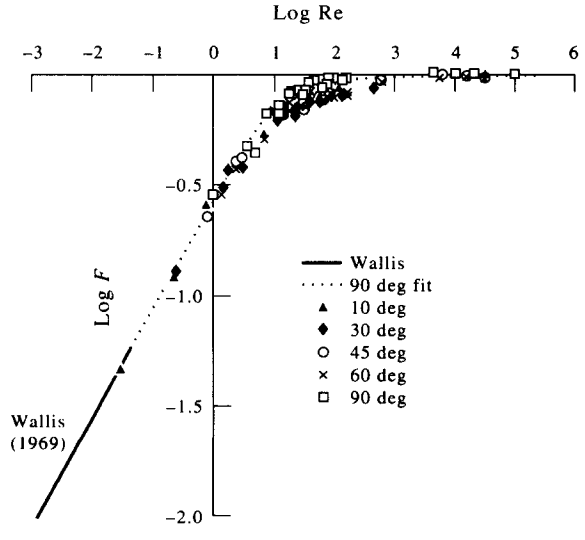

Figure 15. Rise velocity data from figures 7–12 in terms of viscous:inviscid Froude number ratio and bubble Reynolds number with our semi-empirical fit.

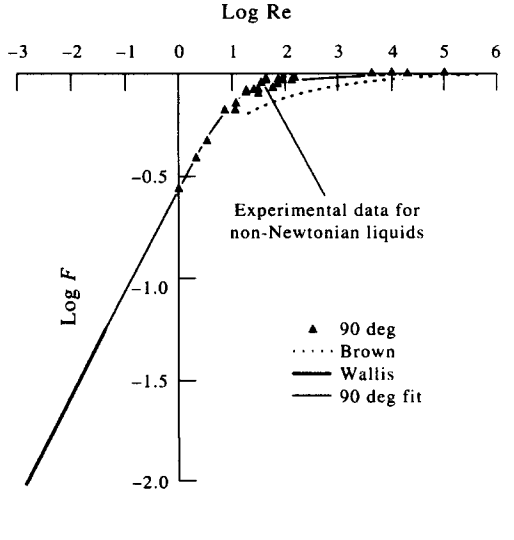

Figure 16. Comparison of [23] with [17] from Wallis (1969) and [21] from Brown (1965).

(c) 3 > Re < 1000

As Re is reduced from the inertially dominated region, the flow field around the bubble becomes more complex, with boundary layers becoming significant. It is noticeable here that in some instances the vertical pipe data provide the highest F values. However, this behaviour arises from the inadequacy of our approximation (see [10]) for voidage ϵ, correlated independently of Eö (see appendix). This shortcoming in ϵ affects our estimate of V' and thus also the value of Fr (Eö, θ, ∞).

The data in figure 15 approximately follow a logarithmic hyperbolic form. Using the asymptotic scalings given by Wallis (1969) and our own expression for high Re leads to the following semi-empirical fit for non-Newtonian effects:

$$\log_{10} F = pz \cdot \left[\left[\frac{\log_{10} \mathrm{Re} + q}{z}\right]^2 + 1\right]^{1/2} + p(\log_{10} \mathrm{Re} + q) \qquad [23]$$

where $p = 0.25$ and $q = -1.08$ are constants equal to the gradient and extrapolated intercept on the log Re axis as found from [17]. Parameter $z = -0.8$ governs the curvature of the correlation line in figure 16 and was chosen to give the best fit over all our data. Simultaneous solution of [23] and [15] in an iterative fashion thus allows the effects of rheology on bubble rise to be characterized. Comparisons are shown for all our data in figures 7–12. The equation agrees best for our 0.045 m tube (Eö $\approx$ 260). For the smaller tubes there is some error such that the predicted Fr are generally too low. In larger tubes the predicted Froude numbers are too high, although this defect is typically less than 10%. These inaccuracies are related to the inadequacies of our simple method for estimating the shear rate manifested as scatter on figure 15 and due to our implicit assumption that elasticity is unimportant here relative to inertial and viscous forces. Also, over the whole range of Eö and for all liquids, Fr ($\theta = 90°$) is underestimated. This shortcoming is seen in figure 16 where [23] only passes through the low Re data points. Referring to figures 7, 10 and 11 we see that the correlation for vertical Fr is best for the high concentration liquids.

7. COMPARISON WITH NEWTONIAN DATA

Figure 17 shows comparisons between our semi-empirical correlation and data for Newtonian liquids from Runge & Wallis (in Wallis 1969) and Weber *et al.* (1986) who both reported data in terms of Fr, Eö and the Mo numbers, rather than in terms of specific diameters, fluids or bubble velocities. The data here were generalized for a pipe diameter of 0.025 cm, surface tension equal to 75 dyn/cm and density of 1.0 g/cm^3 consistent with a viscosity range of 0.001–5.0 Pa s. Rise velocities found under these conditions give rise to a Reynolds number range from 6250 to 0.125. Figure 17 (a)–(d) displays the data for lower viscosities and shows that our formulation underpredicts Fr by less than 10% or so. One exception is shown in figure 17(d) where our model diverges by 20% from data from Weber *et al.* at inclinations close to zero. However, recalling our comments in section 1, we view their zero inclination results with suspicion. Figures 17(e)–(h) contain comparisons for higher viscosities. Above 25° inclination the agreement is excellent and the correlation is shown to be a useful descriptive tool. At shallower angles divergence increases with decreasing inclination, discrepancies caused by the inadequacy of our method for normalizing the data, as depicted in figure 15.

8. CONCLUSIONS AND RECOMMENDATIONS

A semi-empirical correlation has been proposed to describe the rise of long bubbles in inclined ($0 < \theta < 90$) tubes. That part of the correlation scheme applicable to high Re flows is based on bubble rise data taken using pipes with diameters between 0.0216 and 0.178 m. Special attention has been paid to the excess weight of fluid underflowing the bubble nose. This weight term increases with sharpness of the nose region, resulting in higher rise velocities consistent with evidence reported in the literature (Weber *et al.* 1986). Increasing viscosity or increasing surface tension causes the nose region of the bubbles to become blunter and results in lower rise velocities. For viscosity dominated conditions (Re < 1), the rise speed is less dependent on inclination due to the slow drainage of fluid around the nose.

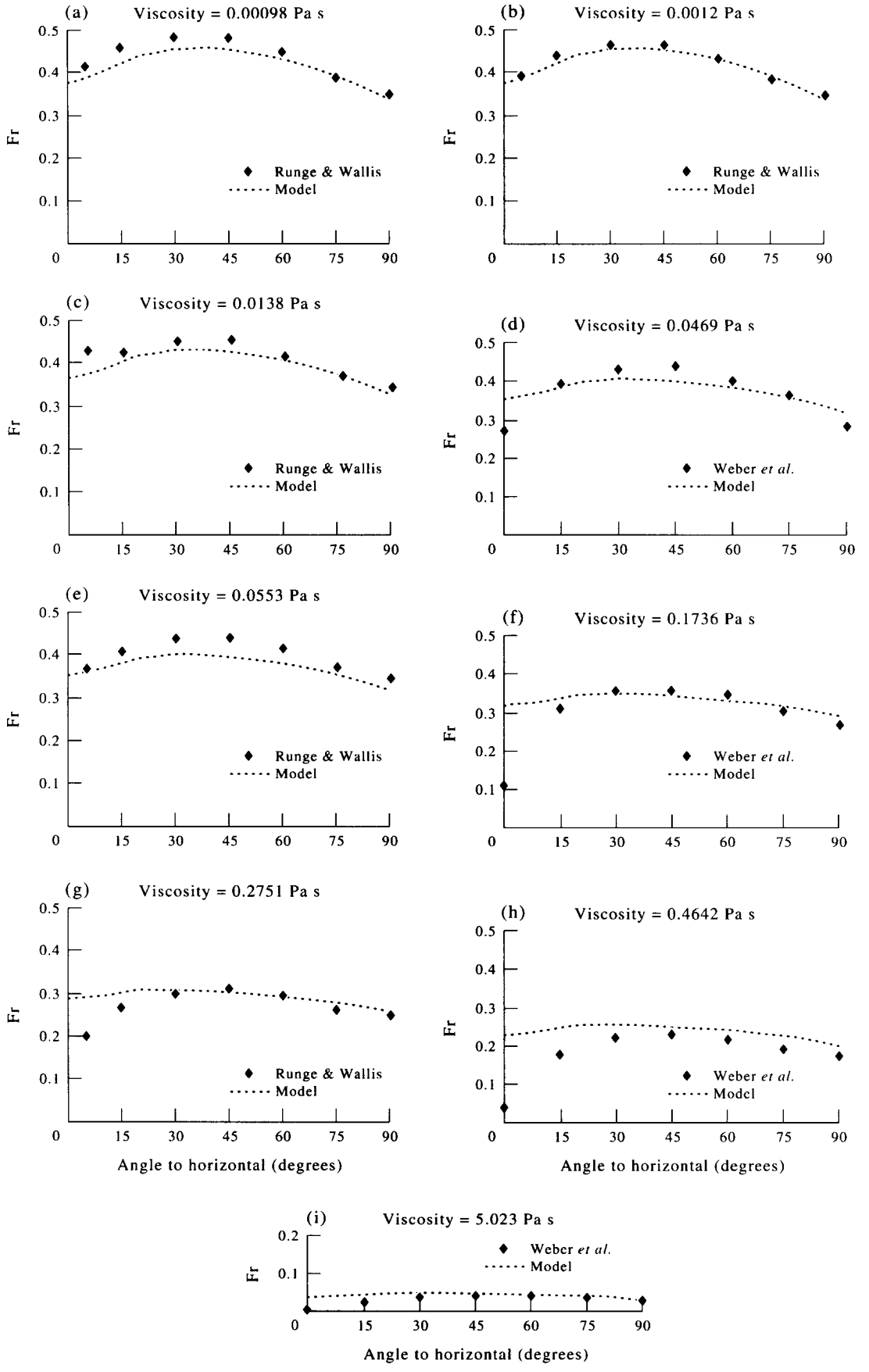

Figure 17. Rise velocity data from Weber *et al.* (1986) and Runge & Wallis (Wallis 1969) compared to our semi-empirical relation. Numbers in legends are viscosities in Pa s.

Inclination dependence of the rise speed in pseudoplastic media ($n = 0.1901$ to 0.485) falls into two zones. In nearly vertical pipes, the bubbles behave as if they were in Newtonian liquid possessing an apparent viscosity appropriate to the local strain-rate near the bubble nose. As the inclination is decreased, the rise velocity decreases and hence also the effective shear rate decreases, resulting in rapidly increasing apparent viscosity. Consequently, Fr approaches zero much more rapidly than in Newtonian liquids. An empirical expression for the effective shear rate dependence on velocity, diameter and inclination has been used to correlate the non-Newtonian Froude number with non-Newtonian bubble Reynolds number. This provides an empirical formula of practical value for pipes above 0.02 m in diameter, based on non-Newtonian data taken using 0.025, 0.045 and 0.07 m diameter pipes, where validation against Newtonian data from literature sources has extended over a broad range of Reynolds numbers from 6250 down to 0.125.

Despite the good agreement between our correlation and Newtonian and non-Newtonian experimental data, only power law rheology has been considered here. Moreover, whilst the steady strain rate response of our test liquids is broadly comparable (figure 5), they exhibit markedly different pouring and handling characteristics. Polyacrylamide is highly visco-elastic (Acharya *et al.* 1977), whereas NaOH modified Carbopol is probably only weekly elastic; indeed, a small Weissenberg effect was observed in preparatory mixing. Visco-elasticity may be expected to be an important factor since the flow around the bubble nose involves unsteady shear and will, therefore, adjust according to the magnitude of the elastic component and extensional viscosity effects; see Barnes *et al.* (1989). Normal fluid stresses, absent in Newtonian fluid flow, might result in significant effects on the shape and velocity of the bubble nose. Yield stress effects have already been mentioned and will lead to zero bubble speeds at inclinations close to the horizontal, especially in smaller diameter tubes. Indeed, there must exist a critical value of the ratio of yield to buoyancy forces for which bubble motion is arrested at all angles. Characterization of thixotropic effects on bubble behaviour is also required.

Other factors which are likely to have important effects on long bubble slip speed are the cross-sectional geometry and the bulk flow of the liquid phase. Geometrical configurations of main practical interest for oilwells are concentric and eccentric annuli in which the liquid flows would display a broad range of velocity profiles upstream of the bubble, causing further readjustment of the interfacial shape (Carew 1993; Carew & Thomas 1995) including displacement of the nose tip away from the pipe wall.

In addition to further experimental work, an improved theoretical basis is now required in order to elucidate the effects of rheological characteristics and upstream velocity profile on the excess volume term. Attention should also be paid to improving the formulation for void fraction ϵ, i.e. the bubble nose shape.

REFERENCES

Acharya, A., Mashelkar, R. A. & Ulbrecht, J. 1977 The mechanics of bubble motion and deformation in non-Newtonian media. *Chem. Engng Sci.* **32,** 863–872.

Barnes, H. A., Hutton, J. F. & Walters, K. 1989 *An Introduction to Rheology*. Elsevier, Amsterdam.

Bendikson, K. H. 1984 An experimental investigation of the motion of long bubbles in inclined tubes. *Int. J. Multiphase Flow* **10,** 467–483.

Benjamin, T. B. 1968 Gravity currents and related phenomena. *J. Fluid Mech.* **31,** 209–248.

Brown R. A. S. 1965 The mechanics of large gas bubbles in tubes: I. Bubble velocities in stagnant liquids. *Can. J. Chem. Engng* **43,** 217–223.

Campos, J. B. L. M. 1991 Mixing induced by air slugs rising in an inclined column of water. *Chem. Engng Sci.* **46,** 2117–2122.

Carew, P. S. 1993 Bubble dynamics of non-Newtonian flows in inclined pipes for the prediction of gas-kicks in oil-wells. Ph.D. thesis, University of Birmingham, England.

Carew, P. S. & Thomas, N. H. 1995 Velocity profile effects on the slug bubble interface shape. Paper in preparation.

Couet, B., Strumolo, G. S. & Ziehl, W. 1987 The effects of fluid properties, inclination and tube geometry on rising bubbles. *3rd Int. Conf. on Multiphase Flow*, The Hague, 18–20 May, paper G3.

Davies, R. M. & Taylor, Sir. G. I. 1950 The mechanics of large bubbles rising through liquids in tubes. *Proc. R. Soc. Lond.* **A200,** 375–390.

Dumitrescu, D. T. 1943 Stromung an einer luftblase im senkrechten rhohr. *Z. angew. Math. Mech.* **23,** 139–149.

Maneri, C. C. & Zuber, N. 1974 An experimental study of plane bubbles rising at inclination. *Int. J. Multiphase Flow* **1,** 623–645.

Mao, Z. & Dukler, A. E. 1991 The motion of Taylor bubbles in vertical tubes: II. Experimental data and simulations for laminar and turbulent flow. *Chem. Engng Sci.* **46,** 2055–2064.

Nguyen, Q. D. & Boger, D. V. 1992 Measuring the flow properties of yield stress fluids. *A. Rev. Fluid Mech.* **24,** 47–88.

Niranjan, K., Hashim, M. A., Pandit, A. B. & Davidson, J. F. 1988 Liquid phase controlled mass transfer from single slugs. *Chem. Engng Sci.* **43,** 1247–1252.

Skelland, A. H. P. 1967 *Non-Newtonian Flow and Heat Transfer.* Wiley, New York.

Wallis, G. B. 1969 *One Dimensional Two-phase Flow.* McGraw–Hill, New York.

Weber, M. E., Alarie, A. & Ryan, M. E. 1986 Velocities of extended bubbles in inclined tubes. *Chem. Engng Sci.* **41,** 2235–2240.

White, E. T. & Beardmore, R. H. 1962 The velocity of single cylindrical air bubbles through liquids contained in vertical tubes. *Chem. Engng Sci.* **17,** 351–361.

Zukoski, E. E. 1966 Influence of viscosity, surface tension and inclination angle on motion of long bubbles in closed tubes. *J. Fluid Mech.* **25,** 821–837.

APPENDIX

Downstream Cross-sectional Geometry

Benjamin (1968), Bendikson (1984) and Campos (1991) all assumed that the shape of the downstream film cross-sectional interface is given by a chordal geometry. In fact, the cross-sectional interface takes up a circular geometry when vertical and will be approximately chordal when the pipe is horizontal. In order to cover the whole range of inclinations we compromise by using a semi-elliptical cross-section [see figure 1(b)]. The elliptical chord intersects the inside pipe circumference at the ends of a horizontal diameter and so has its major axis equal to D. The minor axis, lying in the vertical plane, is given by $D - 2\delta$. From basic geometry we can then see that the wetted perimeter is,

$$P_w = \frac{\pi D}{2} \qquad [A1]$$

the area of a semi-ellipse is given by,

$$A_{se} = \tfrac{1}{2}\pi \frac{D}{2}\left[\frac{D}{2} - \delta\right] \qquad [A2]$$

leading to an expression for the cross-sectional void fraction,

$$\epsilon = 1 - \frac{\delta}{D}. \qquad [A3]$$

In order to evaluate the equilibrium film pressure force, S_2, we need to consider the radial distance between the interface and the centre of pressure. This can be found from a consideration of the moments of area of the ellipse and semi-circle about the lowermost point in a downstream cross-section, leading to the ratio of the distance from the interface to the diameter, ξ

$$\xi = \tfrac{1}{2} - \epsilon - \frac{4\epsilon}{3\pi}. \qquad [A4]$$

Empirical Relationship for Cross-sectional Voidage

To obtain values of ϵ, we proceed as follows:

(i) Use Zukoski's data for u_1 and the continuity equation

$$u_2 = \frac{u_1}{1-\epsilon} \quad [A5]$$

to secure u_2.

(ii) Use the equilibrium of the downstream film flow to write the average wall shear stress over the wetted perimeter

$$\tau_w = \tfrac{1}{2}\rho g D \cdot [1-\epsilon]\sin\theta. \quad [A6]$$

(iii) Introduce the friction factor, C_f, such that

$$\tau_w = \tfrac{1}{2} C_f \rho u_f^2 \quad [A7]$$

where u_f is the average film velocity, relative to the wall, rather than the bubble nose, and is found from u_2 via ϵ

$$u_f = \epsilon u_2. \quad [A8]$$

(iv) Use the empirical friction factor formulae for C_f in terms of the film Reynolds number

$$\mathrm{Re}_f = \frac{\rho u_f d_h}{\mu} = 2\epsilon\ \mathrm{Re} \quad [A9]$$

where

$$d_h = \frac{4 \times \text{flow cross-sectional area}}{\text{wetted perimeter}} = 2D[1-\epsilon]. \quad [A10]$$

Using a simple iterative technique ϵ can be calculated as a function of θ and pipe size (for air and water) as shown in

$$C_f = \frac{16}{\mathrm{Re}_f} \quad \text{for } \mathrm{Re}_f < 2000 \quad [A11]$$

$$C_f = 0.079\ \mathrm{Re}^{-1/4} \quad 2000 < \mathrm{Re}_f < 10^5 \quad [A12]$$

$$\frac{1}{\sqrt{C_f}} = 4\log_{10}[\mathrm{Re}_f\sqrt{C_f}] - 0.4 \quad \mathrm{Re}_f > 10^5 \quad [A13]$$

figure 2 where we have also included our own data for air and water. Since the variation of ϵ is not a strong function of Re (in this case) we have correlated with respect to inclination only. This yields the expression,

$$\epsilon = 0.59 + 0.3031\left[\frac{\theta}{90}\right]^{0.2308} \quad [A14]$$

which is also shown on figure 2 and, in conjunction with [11]–[15], allows calculation of Fr for air and water when Eö > 60.